11th World Congress on Computational Mechanics (WCCM XI)
5th European Conference on Computational Mechanics (ECCM V)
6th European Conference on Computational Fluid Dynamics (ECFD VI)
E. Oñate, J. Oliver and A. Huerta (Eds)

A POSTERIORI ERROR ESTIMATION FOR ADAPTIVE IGA BOUNDARY ELEMENT METHODS

Michael Feischl, Gregor Gantner, and Dirk Praetorius

Institute for Analysis and Scientific Computing, Vienna University of Technology,
Wiedner Hauptstraße 8-10, 1040 Vienna
{michael.feischl, gregor.gantner, dirk.praetorius}@tuwien.ac.at
http://asc.tuwien.ac.at/abem/

Key words: Isogeometric analysis, boundary element method, a posteriori error estimation, adaptive mesh-refinement, NURBS

Abstract. A posteriori error estimation and adaptive mesh-refinement are well-established and important tools for standard boundary element methods (BEM) for polygonal boundaries and piecewise polynomial ansatz functions (see e.g. the seminal work [1] for the derivation of the weighted-residual error estimator and [5] for convergence even with optimal rates). In contrast, the mathematically reliable a posteriori error analysis for isogeometric BEM (IGABEM) has not been considered, yet. In our talk, we aim to shed some light on this gap and to transfer known results on reliable a posteriori error estimators [1, 3] from standard BEM to IGABEM.

As model example serves the weakly-singular integral equation for the 2D Laplacian. For our IGABEM, we employ non-uniform rational B-splines (NURBS). With ϕ denoting the exact solution and Φ_ℓ being the discrete IGABEM solution, we prove that the (numerically computable) Faermann error estimator η_ℓ, proved and analyzed in [3] for standard BEM, provides lower and upper bounds for the (in general, non-computable and unknown) error in the $H^{-1/2}$-energy norm, i.e.,

$$C_{\text{eff}}^{-1}\,\eta_\ell \le |\!|\!| \phi - \Phi_\ell |\!|\!| \le C_{\text{rel}}\,\eta_\ell.$$

In particular, η_ℓ can thus be used to monitor the error decay if the mesh is refined. Moreover, the local contributions of η_ℓ can be used for adaptive IGABEM computations to steer an adaptive algorithm of the form

$$\boxed{\texttt{Solve}} \longrightarrow \boxed{\texttt{Estimate}} \longrightarrow \boxed{\texttt{Mark}} \longrightarrow \boxed{\texttt{Refine}} \tag{1}$$

If compared to uniform mesh refinement, this dramatically reduces the storage requirements as well as the computing time needed to achieve a certain prescribed accuracy.

Acknowledgement. The authors acknowledge support by the Austrian Science Fund (FWF) through the research project P21732 and the doctoral program W1245.

1 INTRODUCTION

Isogeometric analysis (IGA) was introduced in [7] with the intention to significantly reduce the overall time span from the initial design of the geometry to the finite element analysis. This goal was impressively achieved by re-using the shape functions of common *computer aided design* (CAD) models for the finite element (FE) analysis and thus nearly eliminating the process of the so-called mesh-generation. This process, used for classical FE methods, approximates the CAD models by piecewise polynomial meshes suited for common FE solvers and can consume a significant amount of the overall development time [7]. Moreover, subsequent mesh-refinement usually requires a link to the exact geometry stored in the CAD model, which may not be available. This is mentioned in [7] as one of the main reasons why adaptivity is not yet an industrial standard. IGA circumvents these drawbacks, since the exact geometry is automatically preserved during mesh-refinement.

The radically new approach of IGA offers many other advantages over conventional FE analysis. Those include the inherent treatment of variable polynomial degrees on the mesh, a variety of options for mesh refinement, natural inclusion of singularities, and improved stability properties of the resulting FE system due to well-behaving (particularly non-negative) ansatz functions (see Section 3, [7, Section 3]).

Since designers usually construct the surface of the geometry rather than the geometry itself, FE methods require to generate a volume mesh for the use of IGA. This drawback motivates the use of BEM —if applicable to the partial differential equation (PDE) at hand— as it only needs a description and discretization of the surface (boundary) of the computational domain. In this sense, BEM is the *natural* method of IGA. This has been exploited only recently in, e.g., [8, 9] for elastostatic analysis. However, and in contrast to the present work, the mentioned papers rather focus on the application of the method itself than on its analytical properties.

The remainder of the paper is organized as follows. We present the model problem in Section 2, discuss the proposed IGABEM in Section 3, introduce an a posteriori error estimator in Section 4, and finally propose an adaptive algorithm in Section 5. The paper closes with some numerical examples in Section 6, which underline and extend the analytical results of the previous sections.

2 MODEL PROBLEM

Let $\Omega \subset \mathbb{R}^2$ be a bounded Lipschitz domain. We assume that its boundary $\Gamma := \partial\Omega$ can be parametrized by a piecewise smooth path $\gamma : [a, b] \to \Gamma$. Given some Dirichlet data g on Γ, we consider the Laplace-Dirichlet problem

$$-\Delta u = 0 \text{ in } \Omega \text{ with inhomogeneous Dirichlet conditions } u = g \text{ on } \Gamma. \tag{2}$$

The goal is to use BEM to approximate the solution u of the problem above. This motivates the weakly-singular integral equation as a model problem:

$$V\phi(x) := -\frac{1}{2\pi}\int_\Gamma \log|x-y|\phi(y)\,d\Gamma(y) = f(x) \quad \text{for } x \in \Gamma, \tag{3}$$

where V denotes the single-layer integral operator.

Whereas (3) poses an interesting problem on its own, the connection to (2) enters through some particular right-hand side in (3),

$$f = (K+1/2)g \quad \text{with} \quad Kg(x) := \frac{1}{2\pi}\int_\Gamma \frac{(x-y)\cdot\nu(y)}{|x-y|^2}g(y) \tag{4}$$

with K being the so-called double-layer integral operator. Here, $\nu(y)$ denotes the outer unit normal vector of Ω.

The equivalence of (3) and (2) is as follows: If u solves the Laplace-Dirichlet problem (2), the normal flux $\phi = \nabla u \cdot \nu$ solves (3) for $f = (K+1/2)g$. Conversely, if ϕ solves the weakly-singular integral equation (3) for the particular right-hand side $f = (K+1/2)g$, the solution u of (2) reads $u = \widetilde{V}\phi - \widetilde{K}g$, where the single-layer potential $\widetilde{V}$ and the double-layer potential $\widetilde{K}$ formally coincide with the integral operators V resp. K, but are now evaluated in Ω instead of Γ.

The mathematical frame of the formal equations (2)–(3) above requires $u \in H^1(\Omega)$, which is the Sobolev space of square integrable functions whose (weak) gradient is also square integrable. The trace space of $H^1(\Omega)$ reads

$$H^{1/2}(\Gamma) := \big\{u|_\Gamma \,:\, u \in H^1(\Omega)\big\},$$

and contains the Dirichlet data $g \in H^{1/2}(\Gamma)$. Let $H^{-1/2}(\Gamma)$ be the dual space of $H^{1/2}(\Gamma)$ with respect to the extended L^2-scalar product

$$\langle \phi\,,\, v\rangle_{L^2(\Gamma)} := \int_\Gamma \phi v\,d\Gamma,$$

where $\int_\Gamma(\cdot)\,d\Gamma$ denotes integration along the curve. Then, the normal flux $\phi = \nabla u \cdot \nu$ satisfies $\phi \in H^{-1/2}(\Gamma)$ for any (weak) solution $u \in H^1(\Omega)$ of (2).

It is well-known that $V : H^{-1/2}(\Gamma) \to H^{1/2}(\Gamma)$ and $K : H^{1/2}(\Gamma) \to H^{1/2}(\Gamma)$ are continuous and linear operators and that V is additionally symmetric

$$\langle V\phi\,,\,\psi\rangle_{L^2(\Gamma)} = \langle V\psi\,,\,\phi\rangle_{L^2(\Gamma)} \quad \text{for all } \phi,\psi \in H^{-1/2}(\Gamma). \tag{5}$$

In particular, the integral equation (3) is equivalenty stated in the variational formulation

$$\langle V\phi\,,\,\psi\rangle_{L^2(\Gamma)} = \langle f\,,\,\psi\rangle_{L^2(\Gamma)} \quad \text{for all } \psi \in H^{-1/2}(\Gamma). \tag{6}$$

If the domain is appropriately scaled, e.g. its diameter satisfies $\operatorname{diam}(\Omega) < 1$, the operator V is even elliptic

$$\langle \phi \,,\, V\phi \rangle_{L^2(\Gamma)} \geq C_{\rm ell} \, \|\phi\|^2_{H^{-1/2}(\Gamma)} \quad \text{for all } \phi \in H^{-1/2}(\Gamma). \tag{7}$$

Hence, the left-hand side of (6) defines a scalar product on $H^{-1/2}(\Gamma)$, and the Lax-Milgram lemma thus proves existence and uniqueness of the density $\phi \in H^{-1/2}(\Gamma)$. Consequently, the model problem (3) is well-posed for any data $f \in H^{1/2}(\Gamma)$. Moreover, $|\!|\!| \phi |\!|\!|^2 := \langle V\phi \,,\, \phi \rangle_{L^2(\Gamma)}$ defines the equivalent energy norm on $H^{-1/2}(\Gamma)$.

3 IGABEM

We employ a Galerkin discretization of (6) and let $\mathcal{X}$ be a finite-dimensional subspace of $H^{-1/2}(\Gamma)$. Then, the discrete formulation reads

$$\langle V\Phi \,,\, \Psi \rangle_{L^2(\Gamma)} = \langle f \,,\, \Psi \rangle_{L^2(\Gamma)} \quad \text{for all } \Psi \in \mathcal{X}. \tag{8}$$

Again the Lax-Milgram lemma applies and proves existence and uniqueness of the discrete solution $\Phi \in \mathcal{X}$. We note that (8) leads to a linear system of equations with self-adjoint and positive definite matrix, so that Φ is, in fact, computable.

To discretize (6), standard BEM relies on piecewise polynomials, e.g., piecewise constants $\mathcal{X} = \mathcal{P}^0(\mathcal{T})$ for $\mathcal{T} = \{T_1, \dots, T_n\}$ being a partition of Γ into connected boundary elements T_j. Instead, we follow the idea of [8, 9] and consider a NURBS space. Before we give some detailed explanation on how IGABEM works, we introduce some notation.

We consider the parameter domain $[a, b] \subset \mathbb{R}$ and to simplify notation, extend the parametrization $\gamma : \mathbb{R} \to \Gamma$ periodically onto the entire real line. On the parameter domain $[a, b]$, the mesh is controlled via the nodes

$$\big\{ \check{x}_j \,:\, j = 1, \dots, n \big\} \qquad \text{with} \qquad a < \check{x}_1 < \check{x}_2 < \cdots < \check{x}_n = b.$$

Analogously to γ, the nodes are extended periodically to the entire real line

$$\check{x}_{j+n} = \check{x}_j + (b - a) \quad \text{for} \quad j \in \mathbb{Z}$$

and give rise to a mesh on the parameter domain

$$\check{\mathcal{T}} := \{ \check{T}_j \,:\, j \in \mathbb{Z} \} \quad \text{with} \quad \check{T}_j := [\check{x}_{j-1}, \check{x}_j] \quad \text{for} \quad j \in \mathbb{Z}.$$

This partition induces a mesh on Γ by

$$\mathcal{T} := \{T_1, \dots, T_n\} \quad \text{with} \quad T_j := \gamma(\check{T}_j) \quad \text{for all } j = 1, \dots, n.$$

To define NURBS functions on the mesh $\mathcal{T}$ we assign to each node $\check{x}_j$ a corresponding multiplicity $\#\check{x}_j$, which controls the continuity properties of the NURBS basis. This induces a sequence of non decreasing knots $(t_i)_{i=1}^N$ on $[a, b]$ with $\check{x}_1 = t_1 = t_2 = \ldots =$

$t_{\#\check{x}_1}$ and correspondingly for $\check{x}_2, \dots, \check{x}_n$, where $N = \sum_{j=1}^n \#\check{x}_j$. Finally, let $(w_i)_{i=1}^N$ be a sequence of positive weights on these knots. As above, the knot sequence is extended $(b-a)$-periodically to the sequence $(t_i)_{i\in\mathbb{Z}}$ on the real line. The weight sequence is extended to $(w_i)_{i\in\mathbb{Z}}$ by $w_i = w_{i+N}$ for $i \in \mathbb{Z}$.

With this, and the convention $1/0 = 0$, the i-th B-Spline basis function of degree $p \in \mathbb{N}_0$ reads

$$\begin{aligned} B_{i,0} &:= \begin{cases} 1 & \text{in } [t_{i-1}, t_i), \\ 0 & \text{else,} \end{cases} \\ B_{i,p} &:= \frac{t - t_{i-1}}{t_{i-1+p} - t_{i-1}} B_{i,p-1} + \Big(1 - \frac{t - t_i}{t_{i+p} - t_i}\Big) B_{i+1,p-1} \quad \text{for } p \geq 1. \end{aligned} \tag{9}$$

Note that $B_{i,p}$ is always non-negative and vanishes outside of $[t_{i-1}, t_{i+p}]$.

The i-th NURBS basis function of degree p is then a ratio of B-Splines, i.e.,

$$R_{i,p} := \frac{w_i B_{i,p}}{\sum_{k\in\mathbb{Z}} w_k B_{k,p}}, \tag{10}$$

where the apparently infinite series in the denominator is finite due to the local character of the $B_{j,p}$. One can show that the denominator never vanishes, wherefore $R_{i,p}$ is well-defined. The local support of $B_{i,p}$ is preserved in the sense that $R_{i,p}$ vanishes outside $[t_{i-1}, t_{i+p}]$. The NURBS basis defines the trial space $\mathcal{X}$ for the Galerkin problem (8). Given $p \in \mathbb{N}_0$, let

$$\mathcal{X} := \operatorname{span}\{R_{i,p}|_{(a,b)} \circ \gamma^{-1} : i \in \mathbb{Z}\}. \tag{11}$$

Note that $\mathcal{X}$ is finite-dimensional, since indeed $R_{i,p}|_{(a,b)}$ is zero for all but finitely many $i \in \mathbb{Z}$.

There is no general concept of how to choose the knots (t_i) or the weights (w_i). However, if the parametrization γ has a NURBS representation of the form

$$\gamma(t) = \sum_{i\in\mathbb{Z}} C_i R_{i,p}(t) \quad \text{for } t \in \mathbb{R} \tag{12}$$

with some N-periodic control points $(C_i)_{i\in\mathbb{Z}}$ in $\mathbb{R}^2$, it seems valid to choose the same knots and weights for the approximation space $\mathcal{X}$ and the geometry.

4 A POSTERIORI IGABEM ERROR ESTIMATION

According to the Lax-Milgram lemma, the single-layer integral operator is an isomorphism. Let $\|V\|$ resp. $\|V^{-1}\|$ be the corresponding operator norms. By definition, the residual of (8)

$$r := f - V\Phi = V(\phi - \Phi) \in H^{1/2}(\Gamma) \tag{13}$$

satisfies

$$\|V\|^{-1}\,\|r\|_{H^{1/2}(\Gamma)} \le |||\phi - \Phi||| \le \|V^{-1}\|\,\|r\|_{H^{1/2}(\Gamma)}. \tag{14}$$

Hence, an equivalent task for a posteriori error estimation is to monitor the norm of the residual in $H^{1/2}(\Gamma)$.

The trace space $H^{1/2}(\Gamma)$ is either equipped with the trace norm or with the Sobolev-Slobodeckij norm. Both norms are equivalent, and we shall use the Sobolev-Slobodeckij norm. For measurable subsets $\omega \subseteq \Gamma$, one defines the Sobolev-Slobodeckij seminorm by

$$|f|_{H^{1/2}(\omega)} := \int_\omega \int_\omega \frac{|f(x) - f(y)|^2}{|x-y|^2}\, d\Gamma(y)\, d\Gamma(x). \tag{15}$$

With this notation, the Sobolev-Slobodeckij norm on $H^{1/2}(\Gamma)$ reads

$$\|v\|^2_{H^{1/2}(\Gamma)} := \|v\|^2_{L^2(\Gamma)} + |v|^2_{H^{1/2}(\Gamma)} \quad \text{for all } v \in H^{1/2}(\Gamma), \tag{16}$$

and $H^{1/2}(\Gamma)$ can also be characterized by $H^{1/2}(\Gamma) = \big\{v \in L^2(\Gamma) : |v|_{H^{1/2}(\Gamma)} < \infty\big\}$.

Unlike the L^2-norm, the $H^{1/2}$-norm is a nonlocal norm, i.e., for any partition $\mathcal{T}$ it holds

$$|v|^2_{H^{1/2}(\Gamma)} \not\lesssim \sum_{T\in\mathcal{T}} |v|^2_{H^{1/2}(T)} \lesssim |v|^2_{H^{1/2}(\Gamma)}. \tag{17}$$

We refer to a counter example in [2, Section 3] that indeed the lower bound in (17) does not hold in general, i.e., there exists a sequence $v_j \in H^{1/2}(\Gamma)$ with

$$\sum_{T\in\mathcal{T}} |v_j|^2_{H^{1/2}(T)} = 1, \quad \text{while} \quad |v_j|^2_{H^{1/2}(\Gamma)} \xrightarrow{j\to\infty} \infty. \tag{18}$$

For standard BEM with piecewise polynomials, Faermann [3, 4] proposed to consider overlapping domains, e.g., the element patches

$$\omega(T) := \bigcup \big\{T' \in \mathcal{T} : T' \cap T \neq \emptyset\big\} \quad \text{for all } T \in \mathcal{T}. \tag{19}$$

and proved that

$$C_{\rm rel}^{-1}\,\|r\|_{H^{1/2}(\Gamma)} \le \eta_{\mathcal{T}} := \Big(\sum_{T\in\mathcal{T}} |r|^2_{H^{1/2}(\omega(T))}\Big)^{1/2} \le C_{\rm eff}\,\|r\|_{H^{1/2}(\Gamma)}. \tag{20}$$

The heart of the matter in [3] are appropriate Poincaré-Friedrichs inequalities in $H^{1/2}(\Gamma)$ which exploit the Galerkin orthogonality

$$\langle r\,,\,\Psi\rangle_{L^2(\Gamma)} = 0 \quad \text{for all } \Psi \in \mathcal{X} \supset \mathcal{P}^0(\mathcal{T}), \tag{21}$$

which is an immediate consequence of (6) and (8).

Whereas [3] considers arc-length parametrizations γ only, our work [6] generalizes the results to piecewise smooth parametrizations and general NURBS ansatz spaces $\mathcal{X}$ (as defined in the previous section) instead of piecewise polynomials. Note that in the present case, $\mathcal{X}$ does not necessarily contain the piecewise constants $\mathcal{P}^0(\mathcal{T})$, which prevents the use of standard Poincaré-Friedrichs inequalities and requires new ideas.

Our main result reads as follows.

Theorem 1 *Suppose that P is an upper bound for the degree of the B-splines used for the construction of our NURBS space $\mathcal{X}$. Suppose that $W_{\min} > 0$ and $W_{\max} > 0$ are bounds for the weights (w_i) and that the underlying mesh $\mathcal{T}$ of the space satisfies the K-mesh property*

$$\kappa(\mathcal{T}) := \max\Big\{h_T/h_{T'} : T, T' \in \mathcal{T}, T \cap T' \neq \emptyset\Big\} \leq K.$$

Then, the Faermann error estimator $\eta_{\mathcal{T}}$ provides a lower bound (so-called efficiency*) and upper bound (so-called* reliability*) for the IGABEM error* (20)*. The constants $C_{\rm rel}, C_{\rm eff} > 0$ depend only on P,$W_{\min}$,$W_{\max}$, K, and γ.* ■

The practical gain of Theorem 1 is twofold: On the one hand, it allows to monitor the decay of the IGABEM error as the mesh is refined. On the other hand, the definition of $\eta_{\mathcal{T}}$ is local in the sense that it provides some (at least heuristic) information $\eta_{\mathcal{T}}(T) := |r|_{H^{1/2}(\omega(T))}$ about the local error. Therefore, this information can be used to determine, where to refine the underlying mesh $\mathcal{T}$ such that the overall error reduces most effectively. This concept has been successfully applied since the 80s, and it has recently also been mathematically elaborated in the frame of standard BEM [5], where convergence with optimal rates can now be guaranteed.

5 ADAPTIVE IGABEM

This section describes the actual implementation of the adaptive loop (1). For simplicity, we assume that the parametrization γ of Γ can be represented in terms of NURBS basis functions as in (12). We start with the initial partition $\mathcal{T}_0$ of Γ induced by the knots $(t_i^0) = (t_i)$ of γ. Moreover, we use the weights $(w_i^0) := (w_i)$ and control points $(C_i^0) := (C_i)$ of γ to define $\mathcal{X}_0 := \mathcal{X}$ as explained in Section 3. In the following, we abbreviate $\eta_\ell := \eta_{\mathcal{T}_\ell}$, where $\eta_{\mathcal{T}_\ell}$ denotes the Faermann estimator defined in Section 4. The adaptive algorithm then reads as follows

Algorithm 2 Input: *Initial partition $\mathcal{T}_0$, adaptivity parameter $0 < \theta \leq 1$.*
Loop: *for $\ell = 0, 1, 2, \dots$ do (i)–(iv):*

(i) Compute discrete solution $\Phi_\ell \in \mathcal{X}_\ell$ of (8)*.*

(ii) Compute refinement indicators $\eta_\ell(T)$ for all $T \in \mathcal{T}_\ell$.

(iii) Determine set $\mathcal{M}_\ell \subseteq \mathcal{T}_\ell$ of (usually) minimal cardinality such that

$$\theta \sum_{T\in\mathcal{T}_\ell} \eta_\ell(T)^2 \le \sum_{T\in\mathcal{M}_\ell} \eta_\ell(T)^2. \tag{22}$$

(iv) Refine (at least) the marked elements $T \in \mathcal{M}_\ell$ by knot insertion to obtain $(t_i^{\ell+1})$ inducing a mesh $\mathcal{T}_{\ell+1}$. The appropriate weights $(w_i^{\ell+1})$ and control points $(C_i^{\ell+1})$ are calculated such that

$$\mathcal{X}_\ell \subseteq \mathcal{X}_{\ell+1} \quad \text{and} \quad \gamma(t) = \sum_{i\in\mathbb{Z}} C_i^{\ell+1} R_{i,p}^{\ell+1}(t) \quad \text{for } a \le t \le b.$$

Output: *Sequence of estimators η_ℓ and sequence of approximations Φ_ℓ.*

Remark 3 *The computation of the new weights and control points in step* (iv) *of the adaptive algorithm is detailed in [7, Section 2.4].*

The use of the Faermann estimator $\eta_\mathcal{T}$ from Section 4 serves only demonstration purposes. Any other elementwise error indicator as, e.g., $(h-h/2)$-type estimators or residual-type estimators can be used instead.

6 NUMERICAL EXPERIMENTS

In this section we present two numerical examples which underline and empirically validate the theoretical results of Theorem 1.

6.1 Example with smooth solution.

We consider (2)–(3) on the circle with radius $1/10$, center $(0,0)$, and smooth exact solution $u(x,y) = x^2 + 2xy - y^2$ of the PDE formulation (2). The exact solution of the weakly-singular integral equation (3) is the normal derivative of u, i.e.,

$$\phi(x,y) = (\nabla u \cdot \nu)(x,y) = 20(x^2 + 2xy - y^2). \tag{23}$$

The boundary Γ can be parametrized as a NURBS curve with $p = 2$. Figure 1 plots the error $|||\phi - \Phi_\ell|||$ as well as the error estimator η_ℓ over the number of knots for uniform mesh-refinement, i.e., $\theta = 1$. We observe identical slopes for the error and for the error estimator. This underlines the reliability and efficiency of the estimator (20). Moreover, we observe a rate of convergence $\mathcal{O}(N^{-4})$.

6.2 Example with singular solution.

We consider (2)–(3) on the pacman geometry with some reentrant corner from Figure 2, i.e.

$$\Omega := \{R(\cos(\alpha), \sin(\alpha)) : 0 \le R < 1/100, \alpha \in (-3\pi/4, 3\pi/4)\}. \tag{24}$$

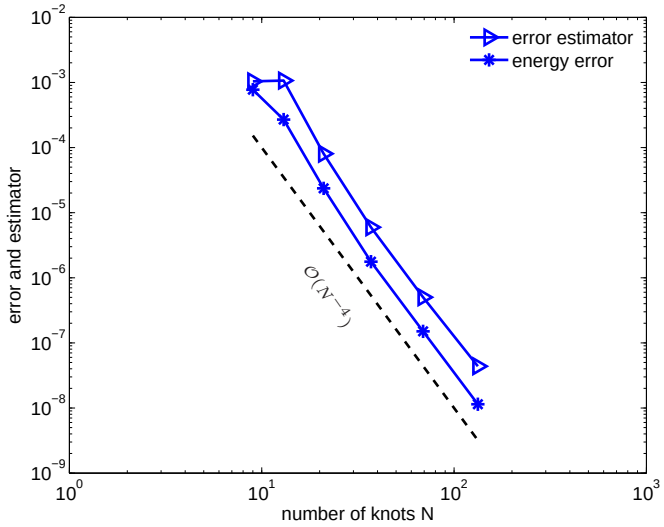

Figure 1: Uniform refinement leads to convergence order $\mathcal{O}(N^{-4})$ for both error and error estimator. In particular, the error estimator is reliable and efficient.

We prescribe the exact solution of (2) by

$$u(x,y) = R^{2/3}\cos(2\alpha/3) \quad \text{in polar coordinates} \quad (x,y) = R(\cos\alpha, \sin\alpha) \tag{25}$$

and note that the exact solution of (3) is the normal derivative $\phi = \nabla u \cdot \nu$. Elementary calculations in polar coordinates reveal

$$\phi(x,y) = \frac{2}{3}\big(w \cdot \nu(x,y)\big) R^{-1/3} \quad \text{with} \quad w = \begin{pmatrix} \cos(\alpha)\cos\left(\frac{2}{3}\alpha\right) + \sin(\alpha)\sin\left(\frac{2}{3}\alpha\right) \\ \sin(\alpha)\cos\left(\frac{2}{3}\alpha\right) - \cos(\alpha)\sin\left(\frac{2}{3}\alpha\right) \end{pmatrix}. \tag{26}$$

In particular, ϕ has a generic singularity at the re-entrant corner $(0,0)$. Figure 3 shows $\phi \circ \gamma$, i.e., the transformation of ϕ to the parameter domain. Again, we parametrize the boundary Γ as a NURBS curve with $p = 2$. Then, we compare uniform refinement $\theta = 1$ and adaptive refinement with $\theta = 0.9$. Figure 4 underlines the clear superiority of the adaptive approach, as we observe a convergence rate of $\mathcal{O}(N^{-5/2})$ compared to $\mathcal{O}(N^{-2/3})$ for uniform mesh-refinement.

REFERENCES

[1] Carstensen, C., Maischak, M., and Stephan, E. P. A posteriori error estimate and h-adaptive algorithm on surfaces for Symm's integral equation. *Numer. Math.* (2001) **20**:197–213.

[2] Carstensen, C. and Faermann, B. Mathematical foundation of a posteriori error estimates and adaptive mesh-refining algorithms for boundary integral equations of the first kind. *Eng. Anal. Bound. Elem.* (2001) **25**:497–509.

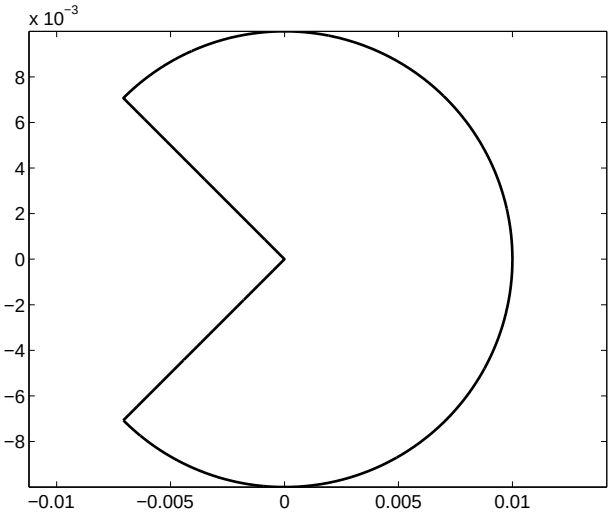

Figure 2: Pacman geometry for the experiment from Section 6.2.

[3] Faermann, B. Localization of the Aronszajn-Slobodeckij norm and application to adaptive boundary element methods, part I. The two-dimensional case. *IMA J. Numer. Anal.* (2000) **20**:203–234.

[4] Faermann, B. Localization of the Aronszajn-Slobodeckij norm and application to adaptive boundary element methods, part II. The three-dimensional case. *Numer. Math.* (2002) **92**:467–499.

[5] Feischl, M., Karkulik, M., Melenk, J. M., and Praetorius, D. Quasi-optimal convergence rate for an adaptive boundary element method. *SIAM J. Numer. Anal.* (2013) **51**:1327–1348.

[6] Feischl, M., Gantner, G., and Praetorius, D. Reliable and efficient a posteriori error estimation for adaptive IGABEM for weakly singular integral equations. Work in progress (2014).

[7] Hughes, T. J. R., Cottrell, J. A., Bazilevs, Y. Isogeometric analysis: CAD, finite elements, NURBS, exact geometry and mesh refinement.. *Comput. Methods Appl. Mech. Engrg.* (2005) **194**:4135-4195.

[8] Simpson, R. N., Bordas, S., Trevelyan, J., Rabczuk, T. A two-dimensional Isogeometric Boundary Element Method for elastostatic analysis *Comput. Methods Appl. Mech. Engrg.* (2012) **209**:87–100.

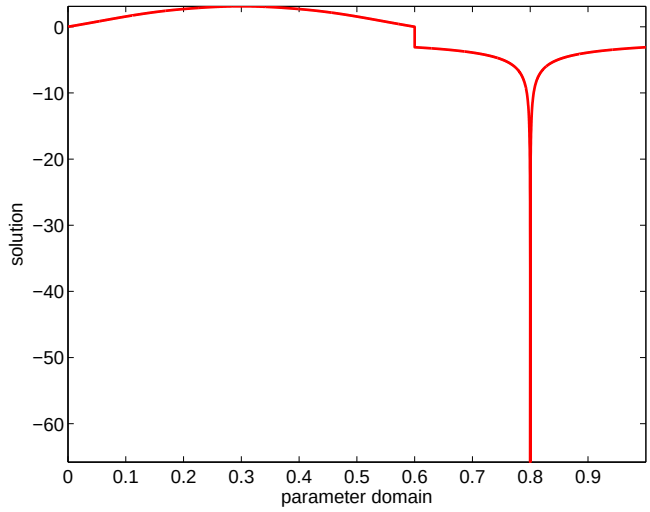

Figure 3: The singular solution $\phi \circ \gamma$ of the experiment from Section 6.2 plotted over the parameter domain. Note that ϕ is singular at $t = 0.8$ which corresponds to the reentrant corner.

[9] Scott, M. A., Simpson, R. N., Evans, J. A., Lipton, S., Bordas, S., Hughes, T. J. R., Sederberg, T. W. Isogeometric boundary element analysis using unstructured T-splines *Comput. Methods Appl. Mech. Engrg.* (2013) **254**:197–221.

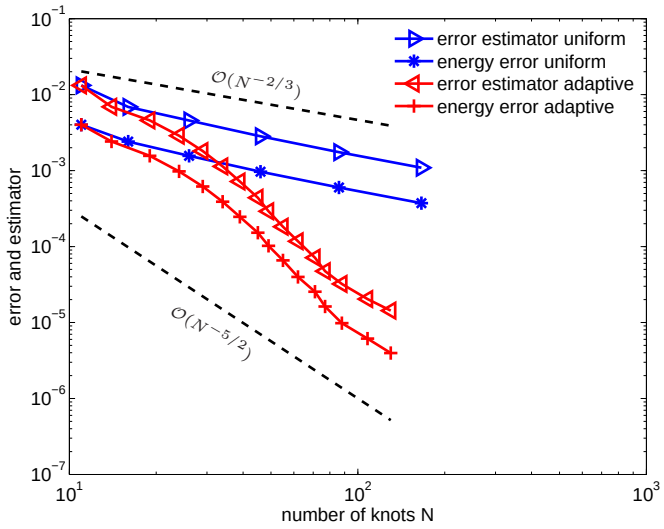

Figure 4: For the singular solution of the experiment from Section 6.2, adaptive refinement leads to faster convergence compared to uniform refinement. Moreover, we observe efficiency and reliability (20) of the error estimator also on adaptive meshes.